Phase-Sensitive Detection of Spin Pumping via the ac Inverse Spin Hall Effect

Mathias Weiler,* Justin M. Shaw, Hans T. Nembach, and Thomas J. Silva
Electromagnetics Division, National Institute of Standards and Technology, Boulder, Colorado 80305, USA
(Received 4 February 2014; published 6 October 2014)

We use a phase-sensitive, quantitative technique to separate inductive and ac inverse spin Hall effect (ISHE) voltages observed in $Ni_{81}Fe_{19}$/normal metal multilayers under the condition of ferromagnetic resonance. For $Ni_{81}Fe_{19}$/Pt thin film bilayers and at microwave frequencies from 7 to 20 GHz, we observe an ac ISHE magnitude that is much larger than that expected from the dc spin Hall angle $\Theta_{SH}^{Pt} = 0.1$. Furthermore, at these frequencies, we find an unexpected, $\approx 110°$ phase of the ac ISHE signal relative to the in-plane component of the resonant magnetization precession. We attribute our findings to a dominant intrinsic ac ISHE in Pt.

DOI: 10.1103/PhysRevLett.113.157204 PACS numbers: 85.75.−d, 72.25.Mk, 75.78.−n, 76.50.+g

Interfacial spin currents enhance the magnetization damping in ferromagnet-normal metal junctions under resonant microwave excitation. This process is called spin pumping [1–3]. For small magnetization precession angles, the dominant contribution to the enhanced damping stems from spin currents that have an ac polarization transversal to the equilibrium magnetization direction. The magnitude of these spin currents is linearly proportional to the dynamic magnetization components. The smaller, nonlinear longitudinally polarized dc spin current component is routinely detected by measuring the dc voltage arising due to the inverse spin Hall effect [4–9] (ISHE) in the normal metal [10–13]. Two fundamental problems need to be solved for a successful detection and quantification of the corresponding ac ISHE voltage [14]. First, any ac ISHE device is also sensitive to inductive signals due to Faraday's law [15] that arise from the precessing magnetization. Second, the presumption that the ISHE is independent of frequency is not necessarily valid, as some theories [16–19] predict a strong frequency dependence. In particular, in the GHz frequency range, theoretical models for two-dimensional electron gases [18,19] based on intrinsic Rashba spin-orbit interaction predict a purely imaginary spin Hall conductivity. Thus, if the ISHE is a superposition of frequency-independent extrinsic (e.g., skew-scattering and side-jump [20]) and frequency-dependent intrinsic processes, dc and ac (inverse) spin Hall angles (ratio of the spin-Hall to charge-conductivity) can be different. At microwave frequencies, we experimentally determine a complex-valued ac inverse spin Hall angle in Pt thin films that is much larger than its dc counterpart.

In the experiments described here, we first separate the inductive and ac ISHE contributions to the ac voltage in $Ni_{81}Fe_{19}$/normal metal thin film stacks and then analyze the magnitude and phase of the ac ISHE. We employ the three-terminal device depicted in Fig. 1(a). Application of an ac voltage to port 1 ($P1$) of the excitation coplanar waveguide (ECPW) generates a microwave magnetic field $\boldsymbol{h}_{mw} \| \boldsymbol{y}$ above its center conductor. The detection coplanar waveguide (DCPW) at $P3$ is mounted at an angle of 90° and with an air gap of 50 μm on top of the ECPW. The DCPW is 50Ω terminated by two rectangular thin-film tabs [$L \times w = (300 \times 100)\ \mu m^2$, center-to-center separation $d = 325\ \mu$m] as depicted in Fig. 1(b). For all samples, the left tab is 15 nm thick $Co_{90}Fe_{10}$ (CoFe in the following) and the right tab is a $Ni_{81}Fe_{19}$ (Py in the following) thin film capped with various normal metal (NM) layers. Each tab has a dc resistance of ≈100Ω. Because the microwave termination for the DCPW is highly symmetric, direct electromagnetic coupling from $P1$ to $P3$ is less than −28 dB up to 20 GHz (see the Supplemental Material [21]). Thus, neither external compensation circuits [27] nor nonlinear excitation schemes [28] to suppress background signals at $P3$ are required.

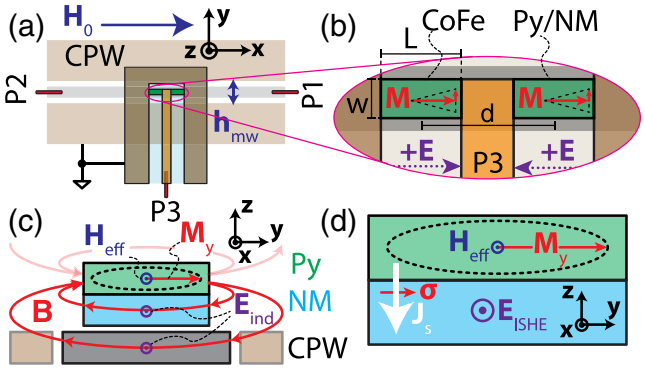

FIG. 1 (color online). (a) Schematic depiction of the excitation CPW (ports $P1$ and $P2$) and detection CPW ($P3$). (b) Close-up of detection CPW showing that the direction of an electric field $\boldsymbol{E}$ that gives rise to a positive voltage at $P3$ is opposite for the two tabs. (c) In the Py/NM tab, the time-varying magnetic flux density $\boldsymbol{B}$ due to the dynamic magnetization component M_y along the $\boldsymbol{y}$ axis causes inductive signals $\boldsymbol{E}_{ind}$ along $\boldsymbol{x}$ in the CPW center conductor and the NM. (d) The dynamic spin current $\boldsymbol{J}_s$ due to M_y gives rise to an ac electric field $\boldsymbol{E}_{ISHE}$ along $\boldsymbol{x}$ by virtue of the inverse spin Hall effect.

We apply a static magnetic field $\boldsymbol{H}_0$ along the $\boldsymbol{x}$ direction. The equilibrium magnetization $\boldsymbol{M}$ is parallel to $\boldsymbol{H}_{\rm eff} \approx \boldsymbol{H}_0$. $\boldsymbol{M}$ precesses around $\boldsymbol{H}_{\rm eff}$ with angular frequency ω in ferromagnetic resonance (FMR). The magnetic flux density $\boldsymbol{B}$ due to the dynamic component M_y threads around the center conductor of the ECPW and the NM of the Py/NM stack in the DCPW, as shown in Fig. 1(c). This time-varying magnetic flux gives rise to electric fields $\boldsymbol{E}_{\rm ind}$ along $\boldsymbol{x}$ in the Py/NM tab and ECPW center conductor according to Faraday's law of induction. The magnitude of the ferromagnetic induction (FMI) voltage $V_{\rm FMI}$ between $P1$ and $P2$ and at $P3$ is approximately [15]

$$V_{\rm FMI} = -i\omega \frac{\mu_0 L t_F}{2} m_y \eta, \tag{1}$$

where μ_0 is the vacuum permeability, $M_y = m_y e^{i\omega t}$, t_F is the ferromagnetic thin film thickness, and $0 \le \eta \le 1$ accounts for attenuation due to nonzero spacing between the Py and ECPW center conductor. ($\eta = 1$ for the Py/NM stack).

To measure $V_{\rm FMI}$ in the ECPW, we measure the complex scattering parameter S_{11} (ratio of ac voltage recorded at $P1$ to ac voltage applied at $P1$) vs H_0 using a vector network analyzer at a fixed microwave frequency f. Figure 2(a) shows data for S_{11} vs H_0 obtained at $f = 9$ GHz for all samples. We first focus on the S_{11} spectra obtained for the Py10/Cu4/Au2 sample (integer numbers are nominal Py/NM layer thicknesses in nm while the CoFe tab for all samples is 15 nm thick). For either polarity of $\boldsymbol{H}_0$, two resonances are observed, one at $\mu_0|H_{\rm res}| \approx 40$ mT and one at $\mu_0|H_{\rm res}| \approx 80$ mT. The dips at smaller absolute $H_{\rm res}$ are due to the FMI detection of the FMR of the CoFe tab, and the dips at larger field magnitudes are due to the FMR of the Py/NM tab, as verified by fitting of the data for $H_{\rm res}$ to the Kittel equation (see the Supplemental Material [21]). Both FMI voltages are at the same phase relative to the excitation field $\boldsymbol{h}_{\rm mw}$ [as evident from the diplike line shape for all resonances in Fig. 2(a)] and symmetric with respect to inversion of the $\boldsymbol{H}_0$ direction. This is in accordance with the detection of an FMI voltage due to $m_y = \chi_{yy} h_y$, where χ_{yy} is a diagonal component of the magnetic susceptibility tensor $\boldsymbol{\chi}$ (see the Supplemental Material [21]), which is even under external magnetic field inversion. The S_{11} data remain qualitatively unchanged for all other samples, with the exception of Py5/Pt10, where the Py FMI signal is below the noise due to both the reduced ferromagnetic volume and the spin-pumping-induced linewidth broadening.

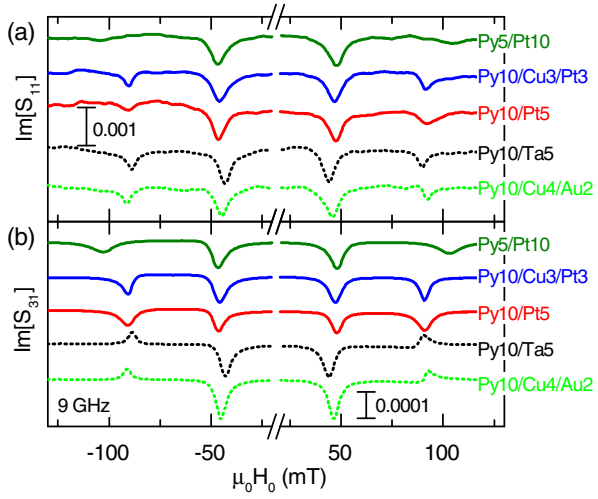

FIG. 2 (color online). (a) Measurements of S_{11} vs H_0 (only Im$[S_{11}]$ shown), which correspond to the inductive signals induced in the ECPW. (b) Simultaneously acquired S_{31} vs H_0 that has both inductive and ac ISHE contributions. The apparent change of sign of the Py/NM resonance for samples with Pt cap (solid lines, "dips") relative to those without Pt cap (dashed lines, "peaks") indicates a dominant noninductive contribution in the samples with Pt cap.

The ratio of ac voltage at $P3$ to ac voltage applied at $P1$ is determined in an S_{31} measurement. On resonance, S_{31} contains both the FMI signal of Eq. (1) and an ISHE signal due to ac spin pumping across the Py/NM interface. The basic idea for the ac ISHE signal generation is sketched in Fig. 1(d): The precessing magnetization is damped in part by an ac spin current $\boldsymbol{J}_{\rm s}$ pumped into the NM layer. M_y gives rise to an ac electric field $\boldsymbol{E}_{\rm ISHE} \propto \boldsymbol{\sigma} \times \boldsymbol{J}_s$ due to the inverse spin Hall effect, where $\boldsymbol{\sigma}$ is the spin-current polarization and $\boldsymbol{J}_{\rm s}$ flows in $-z$ direction. The magnitude of the ac ISHE voltage along $\boldsymbol{x}$ is [14,21]

$$V_{\rm ISHE} = \frac{g_{\uparrow\downarrow}}{2\pi} \omega e \Theta_{\rm SH} \lambda_{\rm SD} \frac{m_z}{M_s} \frac{\tanh(\frac{t_N}{2\lambda_{\rm SD}})}{t_F \sigma_F + t_N \sigma_N} L, \tag{2}$$

where $g_{\uparrow\downarrow}$ is the effective interfacial mixing conductance with units of m^{-2}, e is the elementary charge, $\Theta_{\rm SH}$ is the spin Hall angle of the normal metal, $\lambda_{\rm SD}$ is the spin diffusion length in the NM, M_s is the saturation magnetization, σ_F is the conductivity of the FM, and t_N and σ_N are the thickness and conductivity of the NM, respectively. $V_{\rm ISHE}$ is in phase with the M_y component of $\boldsymbol{M}$ while the $V_{\rm ISHE}$ magnitude is proportional to m_z due to the ellipticity of the precession (Supplemental Material [21]). For circular precession ($m_y = m_z$), there is no qualitative difference between inductive and ac ISHE voltages other than an additional factor of $i\Theta_{\rm SH}$ in $V_{\rm ISHE}$. Hence, for real-valued $\Theta_{\rm SH}$ one excepts a $\pm 90°$ phase shift of $V_{\rm ISHE}$ and $V_{\rm FMI}$, depending on the sign of $\Theta_{\rm SH}$. Furthermore, the ratio $|V_{\rm ISHE}/V_{\rm FMI}|$ is estimated to be on the order of unity for typical Pt/Py bilayers: using $m_y = m_z$, $t_F = t_N = 10$ nm, $\sigma_F = \sigma_N = 3 \times 10^6$ $(\Omega{\rm m})^{-1}$, $M_s = 800$ kA/m, $g_{\uparrow\downarrow} = 3.5 \times 10^{19}$ m^{-2}, $\lambda_{\rm SD} = 1$ nm, and $\Theta_{\rm SH} = 0.1$ as typical material parameters [14] found in our dc ISHE experiments [29], we find $|V_{\rm ISHE}/V_{\rm FMI}| \approx 0.3$. Thus, reliable separation of ac ISHE and FMI signals requires *phase-sensitive* detection.

In Fig. 2(b), we plot the imaginary part of S_{31} acquired simultaneously with S_{11}. Both S parameters are independent of microwave power $10\ \mu\text{W} \leq P_{\text{mw}} \leq 1$ mW applied at $P1$, demonstrating the linearity of both inductive and ac ISHE voltages. In S_{31}, signals of similar amplitude are observed at the resonance fields of both CoFe and Py for all samples. As there is no reasonable expectation for a large ac ISHE in CoFe or Py10/Cu4/Au2, we presume that both resonance signals are due to FMI solely. The fact that an inductive signal is observed for a single CoFe layer is attributed to the nonuniform dynamic magnetization excitation through the film thickness [30]. While the CoFe FMI signal is very similar for all samples and both orientations of H_0, the shape of the Py/NM resonance changes from a peak for Py10/Ta5 and Py10/Cu4/Au2 (dashed lines) to a dip for the samples with Pt caps (solid lines). The apparent phase inversion of the Py10/Ta5 and Py10/Cu4/Au2 S_{31} resonances relative to the CoFe resonances is the result of the inverted polarity for the Py/NM tabs relative to the CoFe tab in the DCPW as indicated in Fig. 1(b). Thus, the data shown in Fig. 2(b) are consistent with a phase shift of approximately 180° correlated with the presence of Pt in the NM stack. The behavior observed for Py10/Ta5 and Py10/Cu4/Au2 is consistent with the observation of a dominant FMI signal in both cases.

To quantify the ac ISHE effect in our devices, we fit the S_{31} data to a linear superposition of two magnetic susceptibilities χ_{CoFe} and χ_{Py} as detailed in the Supplemental Material [21]. We extract from the fits the resonance magnetic field H_{res}, the line width ΔH, the dimensionless magnitude A, and the phase ϕ of the CoFe and Py resonances as a function of frequency for all samples. For all Py resonances, a linear fit of ΔH vs frequency is used to extract the total damping α and the effective spin mixing conductance $g_{\uparrow\downarrow}$. We find $0.88 \times 10^{19}\ \text{m}^{-2} \leq g_{\uparrow\downarrow} \leq 4.11 \times 10^{19}\ \text{m}^{-2}$ as tabulated in the Supplemental Material [21]. Thereby, samples with Pt cap show larger $g_{\uparrow\downarrow}$ than those with Cu/Au and Ta caps.

While the extraction of H_{res} and ΔH from susceptibility measurements is a standard procedure [31], quantification of ac ISHE signals rests on the analysis of A and ϕ, as all other parameters are common to both ac ISHE and FMI. For purely inductive and pure ac ISHE signals, we expect

$$A_{\text{FMI}} e^{i\phi_{\text{FMI}}} = \varepsilon \frac{V_{\text{FMI}}(H_{\text{res}})}{V_1 |\chi_{yy}(H_{\text{res}})|},$$
$$A_{\text{ISHE}} e^{i\phi_{\text{ISHE}}} = \varepsilon \frac{V_{\text{ISHE}}(H_{\text{res}})}{V_1 |\chi_{zy}(H_{\text{res}})|}, \quad (3)$$

respectively. V_1 is the ac voltage applied at $P1$, $|\chi_{zy}(H_{\text{res}})| = |\chi_{yy}(H_{\text{res}})| m_z/m_y$, and the dimensionless factor $0 \leq \varepsilon \leq 1$ accounts for losses in the DCPW. Both A_{FMI} and A_{ISHE} are normalized to the magnetic susceptibility such that they are otherwise independent of the FMR response. If S_{31} can be characterized as a linear superposition of FMI and ac ISHE responses, we can use

$$A e^{i\phi} = A_{\text{ISHE}} \frac{m_z}{m_y} e^{i\phi_{\text{ISHE}}} + A_{\text{FMI}} e^{i\phi_{\text{FMI}}} \quad (4)$$

to deduce the magnitude and phase of the ac ISHE and FMI signals. As detailed in the Supplemental Material [21], ϕ is referenced to the resonance phase of the CoFe tab such that $\phi = 0°$ is expected for a purely FMI signal. This allows us to quantitatively compare ϕ among the different samples.

We plot the extracted A and ϕ as a function of frequency for all investigated Py/NM stacks and both $\boldsymbol{H}_0$ polarities in Figs. 3(a) and 3(b), respectively. We find that A is largest

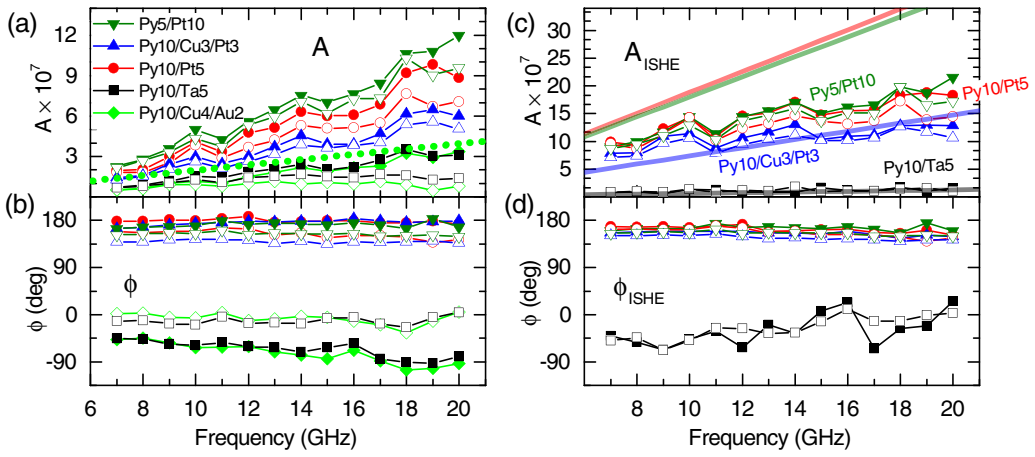

FIG. 3 (color online). (a) The fitted magnitude A for the Py/NM resonances of all samples. Solid symbols correspond to $\boldsymbol{H}_0 \| +\boldsymbol{x}$, and open symbols correspond to $\boldsymbol{H}_0 \| -\boldsymbol{x}$. The dotted line is an estimate for a purely inductive signal for a 10 nm-thick Py film according to Eq. (3). (b) The fitted phase ϕ for all samples. (c),(d) The extracted magnitude and phase of the ac ISHE signal. Solid lines are calculations based on Eq. (3).

for the samples with a Pt cap and maximum for the Py5/Pt10 sample. This would not be expected if the signals were purely FMI. From Eq. (1), one finds $V_{\mathrm{FMI}} \propto t_F$ such that the Py5/Pt10 FMI signal would be smaller than that of Py10/Pt5. We find $\phi \approx 160°$ for all samples capped with Pt, while $-90° \lesssim \phi \lesssim 0°$ for the samples without Pt. The large phase shift and large A caused by the inclusion of a Pt cap strongly suggest an additional noninductive signal source due to the presence of Pt.

Under the presumption that the additional signal is the result of the ac ISHE, we extract the ac ISHE contribution from the variation of A and ϕ between the various samples. The signal from the Py10/Cu4/Au2 sample is effectively due solely to FMI, and we assume that the same FMI signal is present in all Py/NM stacks, except for the Py5/Pt10 sample, where we scale the magnitude of the inductive signal by a factor of one half. By the use of Eq. (4), we obtain A_{ISHE} and ϕ_{ISHE}, shown in Figs. 3(c) and 3(d), respectively. Both A_{ISHE} and ϕ_{ISHE} are even under $\boldsymbol{H}_0$ inversion, consistent with the symmetry of χ_{yy}. In contrast, A_{FMI} and ϕ_{FMI} exhibit an asymmetry under inversion of H_0 [compare open and closed green diamonds in Figs. 3(a) and 3(b)], which is not expected for a signal entirely due to M_y. A possible explanation is the presence of a FMI signal component that is proportional to χ_{zy}, which is odd under field inversion. As we subtract the measured A_{FMI} (Py10/Cu4/Au2) from A to obtain A_{ISHE}, a full quantitative understanding of the FMI signal is however not required.

Equations (1) and (2) predict $\phi_{\mathrm{ISHE}} = 270°$ ($\phi_{\mathrm{ISHE}} = 90°$) for positive (negative) real Θ_{SH}. From Fig. 3(d), we, however, find $\phi_{\mathrm{ISHE}} \approx 160°$ for the samples with a Pt cap and $\phi_{\mathrm{ISHE}} \approx 0°$ for the Py/Ta sample (the large scatter in ϕ_{ISHE} for Py/Ta is attributed to the small A_{ISHE} for this sample). This suggests that Θ_{SH} in these metals is in actuality a complex quantity at microwave frequencies. While no quantitative theory for Pt or Ta exists, this is in qualitative agreement with the observation of a dominantly intrinsic, imaginary ac spin Hall conductivity [19]. A phase shift of the ac ISHE voltage due to spin precession in the external magnetic field [14] is negligible for materials with short spin diffusion lengths such as Pt and Ta. As the measured phase shift persists even for the Py/Cu/Pt sample, interfacial Rashba-like torques [32] can furthermore be excluded as its origin. In the context of the spin Hall effect, our data can be explained by a complex Θ_{SH} with $\arg(\Theta_{\mathrm{SH}}^{\mathrm{Pt}}) = 110°$ and $\arg(\Theta_{\mathrm{SH}}^{\mathrm{Ta}}) \approx -90°$.

We now compare the magnitude of the ac ISHE signal to expectations from Eqs. (1) to (3) using the parameters tabulated in the Supplemental Material [21] and σ_N and σ_F from four-probe dc resistance measurements of bare films. The only uncertain parameters are ε, λ_{SD}, and Θ_{SH}. We first assume that V_{FMI} from Eq. (1) quantitatively accounts for the inductive signal. Then, A_{FMI} for Py/Cu4/Au2 and A_{ISHE} for Py10/Cu3/Pt3 and Py10/Ta5 can be modeled by the use of $\varepsilon = 0.08$, $\lambda_{\mathrm{SD}}^{\mathrm{Pt}} = 1$ nm [33] and $|\Theta_{\mathrm{SH}}^{\mathrm{Pt}}| = 2.5$, $\lambda_{\mathrm{SD}}^{\mathrm{Ta}} = 1$ nm [33], and $|\Theta_{\mathrm{SH}}^{\mathrm{Ta}}| = 0.15$ in Figs. 3(a) (dotted line) and 3(c) (solid lines), respectively. Thus, if Eq. (1) holds true, we observe the largest value for Θ_{SH} in Pt reported to date. However, additional attenuation of the inductive signal for Py/Cu4/Au2 is entirely possible as a result of a nonuniform dynamic magnetization depth profile [30] and due to shunting of the FMI signal by the NM layer that affects the source compliance. A lower limit for Θ_{SH} is obtained by assuming zero losses in the DCPW ($\varepsilon = 1$) resulting in $|\Theta_{\mathrm{SH}}^{\mathrm{Pt}}| = 0.2$ and $|\Theta_{\mathrm{SH}}^{\mathrm{Ta}}| = 0.012$. Thus, even in this limit, we observe a larger $|\Theta_{\mathrm{SH}}^{\mathrm{Pt}}|$ than extrapolated from reported dc values, where $|\Theta_{\mathrm{SH}}^{\mathrm{Pt}}| \leq 0.11$ is typical [34,35]. In previous studies [36–38] $0.0037 \leq |\Theta_{\mathrm{SH}}^{\mathrm{Ta}}| \leq 0.12$ was found, where the huge spread may be due to different crystalline phases of the investigated Ta films. In our dc ISHE experiments on simultaneously deposited layer stacks [29] we find $\Theta_{\mathrm{SH}}^{\mathrm{Pt}} = 0.1$ and $\Theta_{\mathrm{SH}}^{\mathrm{Ta}} = -0.02$. While our measured dc and ac ISHE values are, thus, in reasonable agreement for Ta, the ac ISHE in Pt is found to be much larger than its dc counterpart. Note that Eq. (2) overestimates A_{ISHE} obtained for the two Py/Pt samples by a factor of approximately 2 for parameters where it quantitatively accounts for A_{ISHE} observed in the Py/Cu/Pt sample [see lines in Fig. 3(c)]. This is attributed to interfacial spin flip [39,40] that attenuates the ac ISHE signal in the Py/Pt samples relative to that expected from the damping measurements in the Supplemental Material [21]. In a previous spin-pumping ac ISHE study without phase-sensitive detection [27] in similar Py/NM bilayers, it was also found that the FMI signal in Py/Pt thin films was dominated by the ac ISHE signal. In a study of the ac ISHE in $Y_3Fe_5O_{12}$/Pt by means of parametric excitation [28], the superposition of FMI and ac ISHE signals as well as uncharacterized spin wave modes prevented a quantitative analysis [41,42]. This underlines the importance of phase-sensitive detection and subsequent separation of FMI and ac ISHE signals as carried out in this work.

In summary, we observed ISHE signals due to ac spin pumping in Py/NM multilayers that were discriminated from FMI signals by means of phase-sensitive detection. The magnitude of the ac ISHE signal in Py/Pt exceeds the theoretical prediction [14] even under the assumption of negligible attenuation in the microwave detection circuit. Furthermore, the phase of the ac ISHE signal in these samples is retarded by approximately 110° relative to that expected from theory [14] and assumed in spin Hall spin-torque FMR experiments [43]. While the microscopic origin of both the substantial phase and magnitude of $\Theta_{\mathrm{SH}}^{\mathrm{Pt}}$ at these microwave frequencies (7–20 GHz) is not yet understood, our results are in qualitative agreement with the observation of a dominant intrinsic ac inverse spin Hall effect [19]. Efficient interconversion of charge and spin currents at microwave frequencies is a key requirement for future spintronic devices, such as the recently proposed

spin-Hall-assisted magnetic memory [44]. In order to develop such devices for operation at realistic clock rates, broadband characterization of SHE and ISHE is essential. As such, it could be argued that the dc features of the spin Hall phenomenology are far less important than the microwave properties measured here. Indeed, we propose that Pt is a favorable candidate for such applications due to its surprisingly large ac ISHE.

M. W. acknowledges support from the German Academic Exchange Service (DAAD). Technical assistance by Anthony Kos is greatly appreciated. This work is a contribution of the NIST and is not subject to copyright.

*mathias.weiler@nist.gov

[1] Y. Tserkovnyak, A. Brataas, and G. E. W. Bauer, Phys. Rev. Lett. **88**, 117601 (2002).
[2] Y. Tserkovnyak, A. Brataas, G. E. W. Bauer, and B. I. Halperin, Rev. Mod. Phys. **77**, 1375 (2005).
[3] B. Heinrich, Y. Tserkovnyak, G. Woltersdorf, A. Brataas, R. Urban, and G. E. W. Bauer, Phys. Rev. Lett. **90**, 187601 (2003).
[4] M. Dyakonov and V. Perel, Phys. Lett. **35A**, 459 (1971).
[5] J. E. Hirsch, Phys. Rev. Lett. **83**, 1834 (1999).
[6] S. Zhang, Phys. Rev. Lett. **85**, 393 (2000).
[7] T. Tanaka, H. Kontani, M. Naito, T. Naito, D. S. Hirashima, K. Yamada, and J. Inoue, Phys. Rev. B **77**, 165117 (2008).
[8] G. Y. Guo, S. Murakami, T.-W. Chen, and N. Nagaosa, Phys. Rev. Lett. **100**, 096401 (2008).
[9] H. Kontani, T. Tanaka, D. S. Hirashima, K. Yamada, and J. Inoue, Phys. Rev. Lett. **102**, 016601 (2009).
[10] A. Azevedo, L. H. Vilela Leao, R. L. Rodriguez-Suarez, A. B. Oliveira, and S. M. Rezende, J. Appl. Phys. **97**, 10C715 (2005).
[11] E. Saitoh, M. Ueda, H. Miyajima, and G. Tatara, Appl. Phys. Lett. **88**, 182509 (2006).
[12] O. Mosendz, J. E. Pearson, F. Y. Fradin, G. E. W. Bauer, S. D. Bader, and A. Hoffmann, Phys. Rev. Lett. **104**, 046601 (2010).
[13] K. Ando, S. Takahashi, J. Ieda, Y. Kajiwara, H. Nakayama, T. Yoshino, K. Harii, Y. Fujikawa, M. Matsuo, S. Maekawa, and E. Saitoh, J. Appl. Phys. **109**, 103913 (2011).
[14] H. Jiao and G. E. W. Bauer, Phys. Rev. Lett. **110**, 217602 (2013).
[15] T. J. Silva, C. S. Lee, T. M. Crawford, and C. T. Rogers, J. Appl. Phys. **85**, 7849 (1999).
[16] E. G. Mishchenko, A. V. Shytov, and B. I. Halperin, Phys. Rev. Lett. **93**, 226602 (2004).
[17] O. Entin-Wohlman, A. Aharony, Y. M. Galperin, V. I. Kozub, and V. Vinokur, Phys. Rev. Lett. **95**, 086603 (2005).
[18] C. Grimaldi, E. Cappelluti, and F. Marsiglio, Phys. Rev. Lett. **97**, 066601 (2006).
[19] C. Gorini, R. Raimondi, and P. Schwab, Phys. Rev. Lett. **109**, 246604 (2012).
[20] E. M. Hankiewicz and G. Vignale, Phys. Rev. Lett. **100**, 026602 (2008).
[21] See the Supplemental Material at http://link.aps.org/supplemental/10.1103/PhysRevLett.113.157204, which includes Refs. [22–26].
[22] L. Dreher, M. Weiler, M. Pernpeintner, H. Huebl, R. Gross, M. S. Brandt, and S. T. B. Goennenwein, Phys. Rev. B **86**, 134415 (2012).
[23] H. T. Nembach, T. J. Silva, J. M. Shaw, M. L. Schneider, M. J. Carey, S. Maat, and J. R. Childress, Phys. Rev. B **84**, 054424 (2011).
[24] J. M. Shaw, H. T. Nembach, and T. J. Silva, Phys. Rev. B **87**, 054416 (2013).
[25] J. Mallinson, *The Foundations of Magnetic Recording*, 2nd ed. (Academic Press, San Diego, 1993).
[26] I. Neudecker, G. Woltersdorf, B. Heinrich, T. Okuno, G. Gubbiotti, and C. Back, J. Magn. Magn. Mater. **307**, 148 (2006).
[27] D. Wei, M. Obstbaum, M. Ribow, C. H. Back, and G. Woltersdorf, Nat. Commun. **5**, 3768 (2014).
[28] C. Hahn, G. de Loubens, M. Viret, O. Klein, V. V. Naletov, and J. Ben Youssef, Phys. Rev. Lett. **111**, 217204 (2013).
[29] M. Weiler, J. M. Shaw, H. T. Nembach, and T. J. Silva, arXiv:1409.1290
[30] I. S. Maksymov and M. Kostylev, J. Appl. Phys. **113**, 043927 (2013).
[31] S. S. Kalarickal, P. Krivosik, M. Wu, C. E. Patton, M. L. Schneider, P. Kabos, T. J. Silva, and J. P. Nibarger, J. Appl. Phys. **99**, 093909 (2006).
[32] P. M. Haney, H.-W. Lee, K.-J. Lee, A. Manchon, and M. D. Stiles, Phys. Rev. B **88**, 214417 (2013).
[33] C. T. Boone, H. T. Nembach, J. M. Shaw, and T. J. Silva, J. Appl. Phys. **113**, 153906 (2013).
[34] L. Liu, R. A. Buhrman, and D. C. Ralph, arXiv:1111.3702.
[35] M. Weiler, M. Althammer, M. Schreier, J. Lotze, M. Pernpeintner, S. Meyer, H. Huebl, R. Gross, A. Kamra, J. Xiao, Y. T. Chen, H. Jiao, G. E. W. Bauer, and S. T. B. Goennenwein, Phys. Rev. Lett. **111**, 176601 (2013).
[36] M. Morota, Y. Niimi, K. Ohnishi, D. H. Wei, T. Tanaka, H. Kontani, T. Kimura, and Y. Otani, Phys. Rev. B **83**, 174405 (2011).
[37] L. Liu, C.-F. Pai, Y. Li, H. W. Tseng, D. C. Ralph, and R. A. Buhrman, Science **336**, 555 (2012).
[38] H. L. Wang, C. H. Du, Y. Pu, R. Adur, P. C. Hammel, and F. Y. Yang, Phys. Rev. Lett. **112**, 197201 (2014).
[39] H. Y. T. Nguyen, W. P. Pratt, Jr., and J. Bass, J. Magn. Magn. Mater. **361**, 30 (2014).
[40] J.-C. Rojas-Sánchez, N. Reyren, P. Laczkowski, W. Savero, J.-P. Attané, C. Deranlot, M. Jamet, J.-M. George, L. Vila, and H. Jaffrès, Phys. Rev. Lett. **112**, 106602 (2014).
[41] M. Weiler, H. T. Nembach, J. M. Shaw, and T. J. Silva, arXiv:1401.6407.
[42] C. Hahn, G. de Loubens, M. Viret, O. Klein, V. V. Naletov, and J. Ben Youssef, Phys. Rev. Lett. **112**, 179901(E) (2014).
[43] L. Liu, T. Moriyama, D. C. Ralph, and R. A. Buhrman, Phys. Rev. Lett. **106**, 036601 (2011).
[44] A. van den Brink, S. Cosemans, S. Cornelissen, M. Manfrini, A. Vaysset, W. Van Roy, T. Min, H. J. M. Swagten, and B. Koopmans, Appl. Phys. Lett. **104**, 012403 (2014).